Glider observations of enhanced deep water upwelling at a shelf break canyon: a mechanism for cross-slope carbon and nutrient exchange

M. Porter[1], M. E. Inall[1], J. Hopkins[2], M. R. Palmer[2], A. C. Dale[1], D. Aleynik[1], J. A. Barth[3], C. Mahaffey[5], D. A. Smeed[4]

[1]Scottish Association for Marine Science, Oban, Argyll PA37 1QA, UK

[2] National Oceanography Centre, 6 Brownlow St., Liverpool L3 5DA, UK

[3] College of Oceanic and Atmospheric Sciences, Oregon State University, Corvallis, Oregon, US

[4] National Oceanography Centre, European Way, Southampton SO14 3ZH, UK

[5] Department of Earth, Ocean and Ecological Sciences, University of Liverpool, Liverpool L69 3GP, UK

Corresponding author: Marie Porter (marie.porter@sams.ac.uk)

Key Points:

- Gliders have been used to monitor along canyon flow, identifying upwelled cores
- Intra-seasonal reversals in the slope current have been identified in a long term ADCP record
- Variability in upwelling is associated with variability in the slope current

Abstract

Using underwater gliders we have identified canyon driven upwelling across the Celtic Sea shelf-break, in the vicinity of Whittard Canyon. The presence of this upwelling appears to be tied to the direction and strength of the local slope current, which is in itself highly variable. During typical summer time equatorward flow, an unbalanced pressure gradient force and the resulting disruption of geostrophic flow can lead to upwelling along the main axis of two small shelf break canyons. As the slope current reverts to poleward flow, the upwelling stops and the remnants of the upwelled features are mixed into the local shelf water or advected away from the region. The upwelled features are identified by the presence of sub-pycnocline high salinity water on the shelf, and are upwelled from a depth of 300 m on the slope, thus providing a mechanism for the transport of nutrients across the shelf break onto the shelf.

1 Introduction

Globally, there are over 660 submarine canyons (De Leo et al., 2010). They incise the continental margins of all ocean basins and are known hotspots of enhanced deep-sea sediment and water flux (Savoye et al., 2009), dense water cascades (Canals et al., 2009), benthic biomass (Duineveld et al., 2001) and fishing activity. The complex, irregular topography of the canyons can lead to internal wave generation (Kunze et al., 2002), focusing of internal wave energy (Vlasenko et al., 2016), enhanced diapycnal mixing (Carter and Gregg, 2002), and localized up and downwelling (Allen and Durrieu de Madron, 2009).

In shelf sea environments where the transport of nutrients and carbon between the shelf and open ocean is a crucial component of the Continental Shelf Carbon Pump (Gruber, 2015, Laruelle et al., 2014, Thomas et al., 2004, Tsunogai et al., 1999) the dynamics of cross-slope flow are of particular importance. The shelf seas require a supply of nutrients to fuel their disproportionately

large contribution to global primary productivity (Simpson and Sharples, 2012), and as a means of exporting carbon removed from the atmosphere to the deep ocean below the permanent thermocline. Due to distance from the coast, at the edges of wide shelves such as the NW European shelf this nutrient supply is largely from the open ocean (Proctor et al., 2003).

The Taylor-Proudman theorem states that linear, inviscid and steady geostrophic flow will be constrained to follow f/h contours, thus inhibiting cross-slope exchange (Brink, 1998). However where the assumptions of Taylor-Proudman are violated exchange is possible. The presence of narrow (narrower than the local Rossby radius) canyons can prevent currents from obeying this theorem, potentially leading to an unbalanced pressure gradient force. Depending on the direction of the incident current this may allow for up or downwelling along the axis of the canyon (Allen and Hickey, 2010). On the eastern boundary of a northern hemisphere basin a poleward slope current may drive downwelling, and equatorward slope currents, upwelling. This process can allow submarine canyons on the continental margins to act as conduits between the deep oceans and the shallow seas.

Up and downwelling through canyons, due to ageostrophic flow and the resulting ability of the current to follow the pressure gradient has been identified on shelf breaks world-wide. Examples can be seen on the west coast of North America (Alford and MacCready, 2014) and the west coast of Africa (Hagen, 2001), amongst other places. The phenomenon was first identified by Freeland and Denman (1982), who saw a dense pool of the water at the head of a tributary canyon of the Juan de Fuca canyon, off the west coast of Canada. Freeland and Denman's finding spurred modelling studies (e.g. Allen and Hickey (2010), Jordi et al. (2008), Klinck

(1989)) which when combined with subsequent observational campaigns (e.g. Alford and MacCready (2014), Alvarez et al. (1996)) have highlighted that the up/downwelling potential of a canyon is not simply a function of a large Rossby number on the downstream corner . The local stratification (Allen and Hickey, 2010), the incident current (Allen and Hickey, 2010) and the canyon geometry (Allen and Hickey, 2010, Allen, 2000) also have an impact on the direction and intensity of along canyon-axis flow. Further observational studies have shown that canyons with up/downwelling currents rarely experience either of them as persistent features, with both upwelling and downwelling being seen in a given canyon (Allen and Durrieu de Madron, 2009). Furthermore the occurrences of up/downwelling events in canyons have been observed to be sporadic (Freeland and Denman, 1982).

To further the understanding of seasonal flow dynamics around shelf edge canyons and the role they play in ocean-shelf exchange it is necessary to develop methods that can be used for canyons along the edges of broad shelves and during rough conditions.

In the North East Atlantic the Celtic Sea slope is a non-coastal, continental margin environment. The shelf is wide (circa 300 km) and its slope is a region of highly complex topography, where over 30 canyons incise a 300 km stretch of the shelf edge between the Celtic and Armorican margins (Bourillet et al., 2003). Along the slope is a predominantly poleward slope current, driven largely by the joint effect of baroclinicity and bottom relief (JEBAR) (Huthnance, 1984) and constrained to follow the topography by Taylor-Proudman theorem. In addition to the JEBAR effect this slope current follows SOMA (September/October – March/April) variability (Pingree and Le Cann, 1989, White, 2003, Xu et al., 2015). During the winter months strong

60 prevailing south-westerly winds combined with a meridional density gradient gives a poleward
61 slope current (Huthnance, 1984). However in the summer, relaxing of the south-westerly winds
62 and variability in sea surface height leads to a reversal (Pingree and Le Cann, 1989, Porter et al.,
63 2016).
64
65 Within this study we focus on Whittard Canyon, a large canyon (width of ~55 km at the 2000m
66 contour) on the Celtic Sea slope that is part of the Canyon Marine Conservation Zone (JNCC,
67 2013) with a complicated series of tributary canyons incising the shelf (Figure 1). The main
68 channel is deep, largely oriented in an along-shelf direction and wide when compared to the local
69 first baroclinic Rossby radius of deformation (L_R) ($L_R = \sqrt{(g' \times D)}/f$ where D is the pycnocline
70 depth and $g' = g\,(\rho_1 - \rho_2)/\rho$ where $g = 9.81$ ms^{-2}, ρ_1 the density of the upper (above pycnocline)
71 water, ρ_2 the density of the lower (below pycnocline) water and ρ the mean density), here $L_R \approx 12$
72 km. This large ratio of channel width to L_R allows the flow to stay in geostrophic balance and
73 thus not flow down the pressure gradient. However, a number of the smaller tributary canyons
74 cut across the slope approximately perpendicular to both the slope and the geostrophic slope
75 current. Two of these canyons (A and B on Figure 1) drop from a depth of 200 m at the shelf-
76 break to 3500 m in the bottom of Whittard canyon, over a distance of approximately 5 km. They
77 are narrow, approximately 6-7 km at their 1000 m depth contour, and are approximately half of
78 the local L_R.
79
80 Along the European shelf break the presence of the slope current can be sufficient to cause cross-
81 slope exchange through Ekman veering of near bed currents, which similarly to canyon related
82 geostrophic imbalance can help to move water on shelf during equatorward flow and off shelf

during poleward flow (Kundu, 1976, Huthnance et al., 2009, Simpson and McCandliss, 2013). At the Celtic Sea slope the interaction of the barotropic tide with the irregular and steep (super-critical) slope creates a region of high internal wave activity during the stratified, summer months (Huthnance et al., 2001). Previously it has been shown that cross-slope exchange in this region is dominated through processes related to internal waves, which can be non-linear and propagate from the shelf-break across the shelf towards the coast, transporting mass and energy (Green et al., 2008, Inall et al., 2011). The internal wave energy and the resultant mixing along the shelf break is locally focused in the canyons along this slope (Vlasenko et al., 2016). Furthermore, intense mixing at the shelf break, due to internal waves, is also thought to lead to the exchange phenomenon of "salt lenses", which transport high salinity water over 100 km onto the shelf (Hopkins et al., 2012). During winter, heat loss from the ocean to the atmosphere leads to convective mixing which breaks down surface stratification and ultimately erodes the seasonal thermocline. Consequently the previously described processes, which rely on a stratified environment are diminished or eliminated. The persistence of the slope current year round creates an environment conducive to cross-slope exchange through canyon driven up and downwelling, in addition to Ekman veering beneath the slope current. However, the direct importance of canyons on the Celtic Sea slope as a conduit for cross-shelf exchange has not previously been studied.

Since 2001 the introduction of underwater gliders for hydrographic surveys has allowed us to remotely capture high resolution, spatio-temporal representations of underwater regions (Rudnick et al., 2004). Gliders do not necessarily require the presence of a large ship and they can remain in the water for up to 6 months. The semi-autonomous nature of the gliders and their

106 relative low cost allows for repeated campaigns, giving us easier access to hydrographic data
107 during the winter and in remote regions. Additionally they allow for reactive adaptations in the
108 sampling strategy, producing observational datasets that are highly targeted to a specific
109 objective.
110
111 In this study we show the use of gliders around subsurface, shelf break canyons, highlighting
112 gliders as a data collection instrument that may allow us to ascertain the importance and impact
113 of these canyons on a year round and global basis. We use a moored current profiler to show the
114 seasonality of the slope current on the Celtic Sea slope, indicating that both up and downwelling
115 scenarios are possible. During summer time equatorward flow localized upwelling hotspots are
116 identified, which show a clear decline as the slope current reverses.
117
118 The remainder of the paper is structured as follows: In Section 2 we introduce the data and
119 methods that have been used to provide a spatio-temporal understanding of the hydrographic
120 structure near to two submarine canyons on the Celtic slope. The results of this are then
121 presented in Section 3 followed by a discussion of variability as well as its further impact on
122 nutrient and carbon exchange and the final conclusions in Section 4.

123 **2 Methods and Data**

124 Within this study two Slocum Gliders (Teledyne_Webb, 2010) were flown as a pair, one
125 perpendicular to the shelf break, across the slope (Line 1, Figure 1), and the other parallel to the
126 shelf break (Line 2, Figure 1), (Table 1). The gliders remained in this paired configuration,
127 collecting CTD data for 23 days between the 24th of July and the 15th of August 2012, with the
128 occupation of Line 1 continuing then through until January 2013. This formation allowed us to

observe the properties of the water flowing over the canyons, perpendicular to their main axis, and simultaneously the water shelf-ward of the canyons, parallel with their main axis (Figure 1).

During the 23 days of the canyon-focused glider campaign the gliders collected 248 CTD profiles on Line 1 across the slope and 282 on Line 2 along the shelf, using unpumped SeaBird Electronics CTD sensors (SBE 41). The salinity data collected by these gliders have been cross calibrated with a CTD on the LT1 mooring (yellow diamond in Figure 1) and each other, where appropriate. These data comparisons suggested that there was no sensor drift over the period of this experiment. The calibrated data have been corrected for errors arising from flow speed through the sensors and temperature lag due to thermal inertia within the conductivity cell following the methods of Garau et al. (2011). Each transect was translated onto a 5 km x 5 m grid. Subsequently these grids were interpolated using a Barnes' optimal analysis method (Barnes, 1994), using a horizontal interpolation radius of 15 km, reflecting the autocorrelation of the data and the local internal Rossby radius.

The Celtic Sea slope is subject to strong, non-linear internal tides (Green et al., 2008, Vlasenko et al., 2014). As each glider samples through both time and space it is necessary to mitigate the effects of subsampling or aliasing these internal tides, or at least to be aware of their presence when interpreting the data. In order to most clearly visualize the data and to limit the impact of the internal tide as well as ensuring full data coverage, the transects have been averaged into time means. It is made clear throughout this paper whether the transect being referred to is a single pass or a time mean and over what period averaging has been applied.

In order to contextualize any up/downwelling identified within the canyons it is necessary to know the strength and direction of the local slope current. The velocity structure of the slope current, adjacent to the glider sections, was measured throughout this campaign by two moored 75 kHz long range ADCPs on mooring LT1 (Figure 1, Table 1). The ADCP time series have been filtered using a 71-hour Godin filter, removing the tides. A section of the water column, between 500 m and 1000 m, assumed to be in geostrophic balance, had a mean flow with a bearing of 302°. A clockwise rotation of 58° is therefore applied such that v velocity is aligned locally along the slope (positive poleward) and u locally aligned across-shelf (positive on-shelf).

Through CTD and nutrient profiles in the Petit Sole Canyon (Figure 1) we are able to understand the impact that through canyon upwelling may have on local nutrient exchanges. On these profiles inorganic nutrient concentrations were determined using a Bran and Luebbe QuAAtro five-channel segmented flow nutrient analyzer using standard colorimetric techniques (Grasshoff et al., 2009). Unfiltered seawater samples collected directly from the Niskin bottle were analyzed onboard for concentrations of nitrate plus nitrite (N+N), phosphate (P) and silicate (Si). The limits of detection for N+N, P and Si were 0.1, 0.05 and 0.1 μM and precision was better than 1%.

We will return to the nutrient data in the discussion. First, we will look at the data collected by the gliders on Lines 1 and 2, and the ADCP at LT1.

3 Results

Between the 24th of July and the 15th of August 2012 the depth average current between 500 m and 1000 m at LT1 showed the slope current to be dominated, as expected, by the along-slope

component (Figure 2b). Within this variability, patterns can be identified which show equatorward flow until the 3rd of August, followed by poleward flow until the 13th (Figure 2a).

Next we discuss the glider transects, averaged over the full 23 day campaign and split between the poleward and equatorward phases of the slope current as identified at LT1 (Figure 2a).

3.1 Across-slope hydrography (Line 1)

During this 23 day study the glider on Line 1 completed five transects, which have been averaged to give a campaign-long overview of the hydrographic structure on this line (Figure 3a and b).

We begin by looking at the density structure on the time mean transect. Across the transect the mean pycnocline depth varied between 20 m and 60 m, indicative of summer stratification and a shallow surface mixed layer. Stable stratification throughout the remainder of the water column (mean buoyancy frequency, N = 0.0041 rad s^{-2}) appears to mask the variability in the salinity structure. The large range in temperature compared to that of salinity (Figure 3a and b) gives a temperature dominated stratification profile, allowing salinity to act as a tracer of different water masses.

The time mean temperature and salinity transects show a 3-layer salinity structure (Figure 3a), highlighted in the potential temperature-salinity plot (Figure 4a). The transects are dominated by the presence of Eastern North Atlantic Water (ENAW, practical salinity (S) = 35.23-36.12 potential temperature (Θ) = 8.56-14.86°C (Pollard et al., 1996)), which sits below the seasonal pycnocline at ~100 m to a depth of approximately 700 m. The upper 100 m of this layer contains

198 a tongue of water of subtropical origin ($ENAW_{ST}$ S>35.62 Θ = 12.2 - 14.86°C (Pollard et al.,
199 1996)), whereas the remainder is cooler, fresher and of subpolar origin ($ENAW_{SP}$). While the
200 shallow tongue of $ENAW_{ST}$ is largely isobaric across the transect the deeper $ENAW_{SP}$ upwells
201 towards the slope. Below the ENAW, in the deepest part of the glider section, the upper limit of
202 Mediterranean Water (MEDW, S>35.7 Θ~9.5°C (Harvey, 1982)) can be identified by a deep
203 salinity maximum.

204 **3.2 Along-shelf hydrography (line 2)**

205 Throughout the same 23 day period, six transects were made along Line 2. Line 2 sampled
206 perpendicular to the main axis and near to the head of two cross-slope tributary canyons within
207 Whittard Canyon (A and B in Figure 1). Similar to Line 1, the stable stratification (N = 0.076 rad
208 s^{-2}) and small environmental range of salinity on Line 2 indicate that temperature dominates the
209 density field. The main features are again most clearly identified by salinity contours. (Figure 3c)
210
211 The time mean transect of salinity on Line 2 shows the pycnocline at a depth of approximately
212 80 m, with mixed layer salinity ranging from 35.53 at the surface to 35.62 at around 80 m
213 (Figure 3c). Below the pycnocline the salinity remains largely homogeneous to the bottom, with
214 the exception of two cores of more saline water (S > 35.635). These cores are notably located at
215 the head of the two tributary canyons and appear to show ingress of ENAW onto the shelf
216 (Figures 3c and d and 4b), suggesting that the canyons may experience upwelling.
217
218 In order to further investigate these salinity cores and the potential for canyon enhanced
219 upwelling in this region we have split the data before and after the 4th of August to represent
220 hydrographic conditions when the depth mean flow according to the ADCP data was

equatorward (upwelling favorable) and when it is poleward (downwelling favorable). During each of these periods the tidal phase was similar, with each up/downwelling favorable phase comprising parts of both the spring and neap tide. Consequently it has been assumed that the results observed are not due to spring-neap differences. The glider transects throughout these two periods will be discussed next.

3.3 Equatorward slope current –

Prior to and during the first half of this campaign, up until the 4th of August 2012 the ADCP at LT1 showed that for 29 of the 39 days the water column between 500 m and 1000 m flowed, on average, along the slope towards the equator (Figure 2). The three Line 1 and three Line 2 transects carried out prior to the 4th of August (24th of July - 5th of August) have been averaged, creating one time mean transect for the shelf (Line 1) and one for the slope (Line 2) representing upwelling favorable conditions. These transects show similar structure to the full experiment means, with a 3-layer salinity structure on the slope and two high salinity cores on an otherwise stratified shelf (Figure 5). The presence of 2 salinity cores at the head of the canyons is largely consistent throughout each of the transects averaged within this mean (Figure 6).

Comparison of the water properties in the high salinity cores on Line 2 with the water on Line 1 indicates that the water within the high salinity cores was upwelled from a layer with the same temperature and salinity properties as the water between 150 m and 300 m depth on Line 1 (Figure 5). This estimate is in agreement with the scaling analysis for upwelling depth below shelf break (Z), derived by Allen and Hickey (2010);

$$Z = 1.4\frac{U}{N}\left(\frac{L}{R}\right)^{\frac{1}{2}} \quad (1)$$

where L is the on-shelf deviation of the 200 m isobath in the canyon, 15 km, R is the upstream radius of curvature for the 200 m isobath at the canyon mouth, 3 km, N is the buoyancy frequency (defined previously) and U is the incoming velocity (approximated here by the along slope velocity). Here Z predicts that upwelling starts 100 m below the shelf break depth, which is locally 200 m, giving an upwelling depth of up to 300 m. Alternatively we can compare the depths of isopycnals across the two transects, to infer the upwelling depth. The deepest isopycnal on line 2 is 27.1 kgm^{-3}, which occurs at approximately 200 m (Figure 5). This suggests a shallower upwelling depth than the scaling analysis predicts, however as the lines are not collocated the relative densities are influenced by the effects of mixing during advection. Given the advantages of using the scaling analysis to estimate winter upwelling, when isopycnal comparison is not available we have chosen to continue to use the 300 m upwelling depth, estimated by the scaling analysis.

In this environment the dominance of temperature in the density profiles allows us to use salinity variability along an isopycnal to represent spice, the quantification of temperature and salinity variability along isopycnals (Munk, 1981) in order to infer local mixing and advection regimes. At the edges of the potentially upwelled salinity cores identified above, there are strong along isopycnal salinity gradients (Figure 7). These strong gradients in along isopycnal salinity and therefore implied spice have been used as indicative of the presence of strong fronts and therefore advection as opposed to local mixing (Cole and Rudnick, 2012, Klymak et al., 2015), providing further evidence that these salinity cores are upwelled slope water on the shelf.

3.4 Poleward slope current –

From the 5th of August until mid-November the water column between 500 m and 1000 m depth flowed, on average poleward along the slope (Figure 2).. During the period in which the gliders were in the water (5th August – 15th August) the depth averaged current was in a transition phase and was weaker than later in the year. The four slope and three shelf transects carried out between these dates have been collated creating one time mean transect for Line 2 (on the shelf) and one for Line 1 (on the slope) representing un-favorable upwelling but potentially downwelling favorable conditions (Figure 8). The salinity structure on Line 1 remains similar to the campaign mean, however across Line 2 only vague remnants of the salinity cores can be seen. This transect is also notably fresher than during equatorward flow, with a mean sub-pycnocline salinity of 35.61.

The time mean transect shows that over Canyon A (Figure 1) there was localized high temperature without a concurrent salinity signal (Figure 8). The resulting increase in isopycnal thickness (Figure 8) and simultaneous reduction in along isopycnal salinity gradient (Figure 7) indicates no local fronts, suggesting that that this is a mixed environment (Cole and Rudnick, 2012). However, we cannot discount advection of the salinity cores onshelf through onshelf currents or offshelf due to through canyon downwelling. This termination of the upwelling system is corroborated by the T-S plot which suggests that the water on the slope and the shelf is distinct during this time (Figure 4).

Individual transects give further detail on the termination of the upwelling (Figure 6); the first transect completed under poleward current conditions has notably higher sub-pycnocline salinity than the following transects (Figure 6d). With each pass of the gliders the water freshens,

suggesting that any remnants of the high salinity cores are being removed from the local environment by advection on shelf, entrainment into downwelling or through mixing and are no longer being supplied with high salinity water. Significantly, on Line 1 the hydrographic structure in the shelf break region remained similar throughout the survey, thus the changes seen on the slope do not simply reflect changes in the off-shelf water. The lack of an identifiable salinity core in the first transect under a poleward slope current indicated that the upwelling ceased soon after the reversal in the slope current. This supports the hypothesis that during a poleward slope current there is no upwelling through the canyons, although we do not have the data to ascertain whether a period of downwelling is apparent under these conditions.

Using 2 gliders working perpendicular and parallel to the shelf break in association with a mooring mounted ADCP we have shown that canyons in the Celtic Sea slope cause oceanic water to cross onto the shelf. We see observational evidence that during equatorward flow of the slope current upwelling through the canyons is from the theoretical upwelling depth of 300m. We suggest that under these conditions the canyons can disrupt geostrophic flow and allow water to follow the pressure gradient force onto the shelf.

4 Discussion and Summary

4.1 Variability

Hydrographic glider surveys continuing throughout 2012 on Line 1 combined with continued measurements at LT1 have allowed the variability around the upwelling within these canyons to be assessed.

The switch in the direction of the slope current (depth average of 500 m to 1000 m at LT1) from predominantly equatorward to predominantly poleward reflects the continued variability. The poleward flow, which began in August largely persisted until December 2012, after which time the flow was dominated poleward flow but frequently saw equatorward reversals (5 between the start of December and mid-April). We suggest that this is poleward dominated winter flow is consistent with the well documented SOMA (September/October-March/April) effect (Pingree and Le Cann, 1989; White, 2003; Xu et al., 2015). In conjunction with the observations from this study the SOMA variability indicates that the ability of the canyons to act as conduits between the slope and the shelf is likely to be largely seasonal.

While the data collected here do not allow for the identification of downwelling within the canyon, previous canyon flow studies indicate that this process is likely, but that it is also likely to be weaker than the equivalent upwelling (Allen and Durrieu de Madron, 2009). The seasonality of flow within the canyons may therefore play a role in the continental slope Carbon Pump. When an equatorward slope current occurs in early spring, prior to the spring bloom, upwelling through the canyons may provide deep, nutrient rich water to the shelf. Subsequently, after spring/summer production, the occurrence of a poleward slope current may help to drain the dissolved inorganic carbon (DIC) rich shelf water into the deeper ocean. This potential up and downwelling through the canyons, though asymmetrical, would provide a seasonal rectifier, pumping nutrients onto the shelf in the early summer and pumping DIC off the shelf in autumn and winter.

It is clear throughout the ADCP time series that small scale variability in slope current direction, atypical for the specific SOMA season is frequent (Figure 2). During the record there are 8 periods of equatorward flow lasting between 3 and 24 days which have the potential to drive through canyon upwelling. Consequently, intermittent upwelling may also be important during the winter, when the hydrographic properties of the water impacting the canyons are different to during the observed, summer period. In early December when the prevailing poleward slope current was briefly interrupted by equatorward flow during which time one glider, SG156 (Table 1) was sampling on Line 1. Throughout this period the upwelling depth predicted by equation (1) had deepened slightly to 320 m. Glider transects during this time suggest that the water at the depth had increased in salinity (Figure 9). At the estimated upwelling depth there is an increased incidence of $ENAW_{ST}$ and consequently a change in the dominant upwelled water mass when compared to the transects studied in detail within this study.

Not only is the slope current seasonally variable, but it has notable variability in both its strength and direction on an inter-annual basis. It has previously been shown that it is possible to estimate the range in the velocity of the slope current using altimetry data (Xu et al, 2015) without using direct measurements. Xu et al (2015) showed that altimetry derived geostrophic currents along the European slope can explain over 50% of the variability of the currents observed within ADCPs and lagrangian floats. The clear variability seen within this altimetry study indicates that on the Celtic Sea it is necessary to at least estimate the state of the slope current before inferring upwelling favorable conditions.

353 **4.2 Impact on nutrient flux**

354 The onset of an equatorward slope current in March/April will often precede the spring bloom of
355 phytoplankton on the shelf (Rees et al., 1999). The occurrence of canyon based upwelling
356 associated with the slope current provides a mechanism of cross slope flow, and therefore a
357 pathway for nutrient advection onto the shelf, during a time when a cross slope flow may
358 otherwise be largely absent (Hydes et al., 2001).

359

360 On the 24th of June 2012, a transect of 4 CTD profiles (Figure 1) was sampled for nutrients along
361 the axis of the Petite Sole canyon (Vlasenko et al., 2016) adjacent to the canyons A and B in this
362 study. Linear regressions suggested that the variance of the profiles of nitrate + nitrite (N+N),
363 silicate (Si) and phosphate (P) was well explained by the potential density with mean R^2 of 0.96
364 for N+N, 0.82 for Si and 0.91 for P ($p<0.001$ for all three regressions). Assuming this
365 relationship between density and the nutrient concentration is consistent between the 3 adjacent
366 canyons we can use this to infer chemical properties of the upwelled water.

367

368 While Figure 6 suggests that the density may be largely temperature compensated, it is clear that
369 there is variability in the density structure associated with the cooler and high salinity upwelled
370 salinity cores. During upwelling favorable conditions the sub-pycnocline water is approximately
371 0.1 kg m^{-3} denser than otherwise (Figure 10a). Given the density-nutrient relationship seen in the
372 Petite Sole canyon this would imply that water with elevated N+N (as well as Si and P, which
373 are not shown) has been advected onto the shelf (Figure 10a), with an increase of up to 2 μM of
374 N+N. Correspondingly we can see that at C4 (48.4°N, 9.6°W), the deepest nutrient station, the
375 N+N concentrations are higher at 300 m, the maximum extent of the upwelling, than at the
376 bottom depths of the shelf station (Figure 10b).

This process is likely to persist throughout the summer, adding to the pathways for nutrients onto the shelf during a period when nutrient concentrations are depleted in surface waters due to biological consumption. Subsequently, potential downwelling which may be predominant in the autumn and winter would provide a pathway to remove DIC contained in the shelf water to the deeper ocean, after the summer bloom. Throughout this period, intermittent upwelling may provide winter time nutrient pathways.

4.3 Summary

In this paper we have used hydrographic data from 2 gliders on the Celtic Sea slope, with further context provided by a slope based, moored ADCP. We have demonstrated that in typically summer time conditions, where the slope current is equatorward, canyons in the slope can work as a pathway for upwelling of nutrient enriched slope water onto the shelf. Conversely in typically winter time conditions, a poleward slope current, the upwelling is no longer seen.

The hydrographic surveys presented here add to the current body of work focusing on canyon driven upwelling. We have highlighted that short-term (order of 1 week) yet sustained changes in the direction of the currents incident on the canyon can drive or prevent this type of upwelling. It is clear that the gliders used within this study allow for a detailed description of the variability in these flows without the need for large and inherently expensive ship-based observational campaigns.

The seasonal reversal in the slope current, the SOMA effect, which leads to the seasonality of the upwelling is in itself variable on a year to year basis. Such intra-annual variability is likely to be

400 further reflected in the variability of the upwelling. Changes in the approximated upwelling
401 depth associated with the incident flow speed suggest that when equatorward flow is weak there
402 would be insufficient upwelling to draw up water from deeper than the shelf break (Allen and
403 Hickey, 2010), leading to a cessation of upwelling even under an equatorward slope current. This
404 prediction, based on a theoretical calculation (equation 1), requires further observations or
405 detailed modelling efforts to ascertain how the strength of the slope current influences the
406 strength or even the presence of upwelling through the canyons.

407 **Acknowledgments and Data**

408 This study was funded by the UK Natural Environment Research Council project Fluxes Across
409 Sloping Topography of the North East Atlantic (FASTNEt) (NE/I030151/1). M. Porter was
410 funded to visit J.Barth through a SAGES PECRE grant. We thank the crew and scientists of the
411 D376 for the glider and mooring deployments and all involved with nutrient collection as well as
412 glider recoveries and piloting.

413

414 The data are all available on request from the British Oceanographic Data Centre
415 (http://www.bodc.ac.uk/projects/uk/fastnet/data_inventories/) or through contacting the relevant
416 data manager listed therein.

417

418

419 **References**

420

421 ALFORD, M. H. & MACCREADY, P. 2014. Flow and mixing in Juan de Fuca Canyon, Washington. *Geophysical*
422 *Research Letters,* 41**,** 1608-1615.
423 ALLEN, S. & DURRIEU DE MADRON, X. 2009. A review of the role of submarine canyons in deep-ocean
424 exchange with the shelf. *Ocean science,* 5**,** 607-620.
425 ALLEN, S. E. 2000. On subinertial flow in submarine canyons: Effect of geometry. *Atmospheric Science Program*.
426 ALLEN, S. E. & HICKEY, B. 2010. Dynamics of advection-driven upwelling over a shelf break submarine canyon.
427 *Journal of Geophysical Research: Oceans (1978–2012),* 115.

ALVAREZ, A., TINTORÉ, J. & SABATÉS, A. 1996. Flow modification and shelf-slope exchange induced by a submarine canyon off the northeast Spanish coast. *JOURNAL OF GEOPHYSICAL RESEARCH-ALL SERIES-,* 101**,** 12,043-12,055.

BARNES, S. L. 1994. Applications of the Barnes objective analysis scheme. Part II: Improving derivative estimates. *Journal of Atmospheric and Oceanic Technology,* 11**,** 1449-1458.

BOURILLET, J. F., REYNAUD, J. Y., BALTZER, A. & ZARAGOSI, S. 2003. The 'Fleuve Manche': the submarine sedimentary features from the outer shelf to the deep-sea fans. *Journal of Quaternary Science,* 18**,** 261-282.

BRINK, K. H. 1998. Deep-sea forcing and exchange processes. In: A. Robinson and K. H. Brink (eds) The sea, vol. 10: the global coastal ocean. *The sea.* New York.

CANALS, M., DANOVARO, R., HEUSSNER, S., LYKOUSIS, V., PUIG, P., TRINCARDI, F., CALAFAT, A., DURRIEU DE MADRON, X., PALANQUES, A. & SANCHEZ-VIDAL, A. 2009. Cascades in Mediterranean submarine grand canyons. *Oceanography,* 22**,** 26-43.

CARTER, G. S. & GREGG, M. C. 2002. Intense, variable mixing near the head of Monterey Submarine Canyon. *Journal of physical oceanography,* 32**,** 3145-3165.

COLE, S. T. & RUDNICK, D. L. 2012. The spatial distribution and annual cycle of upper ocean thermohaline structure. *Journal of Geophysical Research: Oceans,* 117**,** C02027.

DE LEO, F. C., SMITH, C. R., ROWDEN, A. A., BOWDEN, D. A. & CLARK, M. R. 2010. Submarine canyons: hotspots of benthic biomass and productivity in the deep sea. *Proceedings of the Royal Society of London B: Biological Sciences***,** rspb20100462.

DUINEVELD, G., LAVALEYE, M., BERGHUIS, E. & DE WILDE, P. 2001. Activity and composition of the benthic fauna in the Whittard Canyon and the adjacent continental slope (NE Atlantic). *Oceanologica Acta,* 24**,** 69-83.

FREELAND, H. & DENMAN, K. 1982. A topographically controlled upwelling center off southern Vancouver Island. *Journal of Marine Research,* 40**,** 1069-1093.

GARAU, B., RUIZ, S., ZHANG, W. G., PASCUAL, A., HESLOP, E., KERFOOT, J. & TINTORÉ, J. 2011. Thermal lag correction on Slocum CTD glider data. *Journal of Atmospheric and Oceanic Technology,* 28**,** 1065-1071.

GRASSHOFF, K., KREMLING, K. & EHRHARDT, M. 2009. *Methods of seawater analysis*, John Wiley & Sons.

GREEN, J. M., SIMPSON, J. H., LEGG, S. & PALMER, M. R. 2008. Internal waves, baroclinic energy fluxes and mixing at the European shelf edge. *Continental Shelf Research,* 28**,** 937-950.

GRUBER, N. 2015. Ocean biogeochemistry: Carbon at the coastal interface. *Nature,* 517**,** 148-149.

HAGEN, E. 2001. Northwest African upwelling scenario. *Oceanologica Acta,* 24**,** 113-128.

HARVEY, J. 1982. θ-S relationships and water masses in the eastern North Atlantic. *Deep Sea Research Part A. Oceanographic Research Papers,* 29**,** 1021-1033.

HOPKINS, J., SHARPLES, J. & HUTHNANCE, J. 2012. On-shelf transport of slope water lenses within the seasonal pycnocline. *Geophysical Research Letters,* 39.

HUTHNANCE, J. 1984. Slope currents and "JEBAR". *Journal of Physical Oceanography,* 14**,** 795-810.

HUTHNANCE, J. M., COELHO, H., GRIFFITHS, C. R., KNIGHT, P. J., REES, A. P., SINHA, B., VANGRIESHEIM, A., WHITE, M. & CHATWIN, P. G. 2001. Physical structures, advection and mixing in the region of Goban spur. *Deep Sea Research Part II: Topical Studies in Oceanography,* 48**,** 2979-3021.

HUTHNANCE, J. M., HOLT, J. T. & WAKELIN, S. L. 2009. Deep ocean exchange with west-European shelf seas. *Ocean science,* 5**,** 621-634.

HYDES, D. J., LE GALL, A. C., MILLER, A. E. J., BROCKMANN, U., RAABE, T., HOLLEY, S., ALVAREZ-SALGADO, X., ANTIA, A., BALZER, W., CHOU, L., ELSKENS, M., HELDER, W., JOINT, I. & ORREN, M. 2001. Supply and demand of nutrients and dissolved organic matter at and across the NW European shelf break in relation to hydrography and biogeochemical activity. *Deep Sea Research Part II: Topical Studies in Oceanography,* 48**,** 3023-3047.

INALL, M., ALEYNIK, D., BOYD, T., PALMER, M. & SHARPLES, J. 2011. Internal tide coherence and decay over a wide shelf sea. *Geophysical Research Letters,* 38.

JNCC 2013. MCZ Site Summary Document: The Canyons MCZ. Version 4.0, November 2013. JNCC, UK. Available from: (jncc.defra.gov.uk/marineprotectedareas).

JORDI, A., KLINCK, J., BASTERRETXEA, G., ORFILA, A. & TINTORÉ, J. 2008. Estimation of shelf-slope exchanges induced by frontal instability near submarine canyons. *Journal of Geophysical Research: Oceans,* 113.

KLINCK, J. M. 1989. Geostrophic adjustment over submarine canyons. *Journal of Geophysical Research: Oceans,* 94**,** 6133-6144.
KLYMAK, J. M., CRAWFORD, W., ALFORD, M. H., MACKINNON, J. A. & PINKEL, R. 2015. Along-isopycnal variability of spice in the North Pacific. *Journal of Geophysical Research: Oceans,* 120**,** 2287-2307.
KUNDU, P. K. 1976. Ekman veering observed near the ocean bottom. *Journal of physical oceanography,* 6**,** 238-242.
KUNZE, E., ROSENFELD, L. K., CARTER, G. S. & GREGG, M. C. 2002. Internal Waves in Monterey Submarine Canyon. *Journal of physical oceanography,* 32**,** 1890-1913.
LARUELLE, G. G., LAUERWALD, R., PFEIL, B. & REGNIER, P. 2014. Regionalized global budget of the CO2 exchange at the air-water interface in continental shelf seas. *Global Biogeochemical Cycles,* 28**,** 2014GB004832.
MUNK, W. 1981. Internal waves and small-scale processes. *Evolution of physical oceanography***,** 264-291.
PINGREE, R. & LE CANN, B. 1989. Celtic and Armorican slope and shelf residual currents. *Progress in Oceanography,* 23**,** 303-338.
POLLARD, R., GRIFFTTHS, M., CUNNINGHAM, S., READ, J., PÉREZ, F. F. & RÍOS, A. F. 1996. Vivaldi 1991-A study of the formation, circulation and ventilation of Eastern North Atlantic Central Water. *Progress in Oceanography,* 37**,** 167-192.
PORTER, M., INALL, M., GREEN, J., SIMPSON, J., DALE, A. & MILLER, P. 2016. Drifter observations in the summer time bay of Biscay slope current. *Journal of Marine Systems*.
PROCTOR, R., HOLT, J. T., ALLEN, J. I. & BLACKFORD, J. 2003. Nutrient fluxes and budgets for the North West European Shelf from a three-dimensional model. *Science of The Total Environment,* 314–316**,** 769-785.
REES, A. P., JOINT, I. & DONALD, K. M. 1999. Early spring bloom phytoplankton-nutrient dynamics at the Celtic Sea Shelf Edge. *Deep Sea Research Part I: Oceanographic Research Papers,* 46**,** 483-510.
RUDNICK, D. L., DAVIS, R. E., ERIKSEN, C. C., FRATANTONI, D. M. & PERRY, M. J. 2004. Underwater gliders for ocean research. *Marine Technology Society Journal,* 38**,** 73-84.
SAVOYE, B., BABONNEAU, N., DENNIELOU, B. & BEZ, M. 2009. Geological overview of the Angola–Congo margin, the Congo deep-sea fan and its submarine valleys. *Deep Sea Research Part II: Topical Studies in Oceanography,* 56**,** 2169-2182.
SIMPSON, J. H. & MCCANDLISS, R. R. 2013. "The Ekman Drain": a conduit to the deep ocean for shelf material. *Ocean Dynamics,* 63**,** 1063-1072.
SIMPSON, J. H. & SHARPLES, J. 2012. *Introduction to the physical and biological oceanography of shelf seas*, Cambridge University Press.
TELEDYNE_WEBB. 2010. Available: http://www.webbresearch.com/slocumglider.aspx.
THOMAS, H., BOZEC, Y., ELKALAY, K. & DE BAAR, H. J. W. 2004. Enhanced Open Ocean Storage of CO2 from Shelf Sea Pumping. *Science,* 304**,** 1005-1008.
TSUNOGAI, S., WATANABE, S. & SATO, T. 1999. Is there a "continental shelf pump" for the absorption of atmospheric CO2? *Tellus B,* 51**,** 701-712.
VLASENKO, V., STASHCHUK, N., INALL, M. E. & HOPKINS, J. E. 2014. Tidal energy conversion in a global hot spot: On the 3-D dynamics of baroclinic tides at the Celtic Sea shelf break. *Journal of Geophysical Research: Oceans,* 119**,** 3249-3265.
VLASENKO, V., STASHCHUK, N., INALL, M. E., PORTER, M. & ALEYNIK, D. 2016. Focusing of baroclinic tidal energy in a canyon. *Journal of Geophysical Research: Oceans*.
WHITE, M. 2003. Comparison of near seabed currents at two locations in the Porcupine Sea Bight—implications for benthic fauna. *Journal of the Marine Biological Association of the UK,* 83**,** 683-686.
XU, W., MILLER, P. I., QUARTLY, G. D. & PINGREE, R. D. 2015. Seasonality and interannual variability of the European Slope Current from 20years of altimeter data compared with in situ measurements. *Remote Sensing of Environment,* 162**,** 196-207.

Figure captions

Figure 1:

536 Bathymetric maps of the study region. The topography data is from Etopo1, with superimposed
537 multibeam (GSI Dublin) data where available in (b). In (a) the 200 m, 300 m, 500 m, 1000 m,
538 2000 m, 3000 m, and 4000 m isobaths picked out by black contours. (b) shows the glider
539 transects used within this study, indicated by the red lines and the location of the ADCP mooring
540 is shown by the yellow diamond. The canyons referred to in the text are labelled A and B. The
541 CTD transect is shown by blue circles.

542 Figure 2:

543 (a) The along-slope component velocity of the depth average from 500 m-1000 m from the
544 ADCP at LT1. Poleward flow is signified by positive velocity and equatorward by negative. The
545 dashed black line shows August the 5^{th} , the short, solid black line indicates the glider canyon
546 campaign and the dashed orange boxes highlight equatorward flow. (b) shows the directions
547 (angle) and frequency (spoke length) as well as the speed (shading) of the 500 m – 1000 m depth
548 average current at LT1. This current rose covers that same period as (a).

549 Figure 3: (a) and (b) are from Line 1 (across slope) and show the time mean transects between
550 24^{th} July and 15^{th} August from glider 330, while (c) and (d) show the same time means from
551 Line 2 (along slope), using glider 194. Figures (a) and (c) show the salinity, (b) and (d) the
552 temperature. The black contours indicate the density.

553 Figure 4:

554 Potential temperature and salinity plots for (a) all profiles on line 1 and (b) all profiles on line 2.
555 The plots are coloured by depth, it should be noted that the colorbar scale is different on each
556 plot. The red dashed line shows the properties of the $ENAW_{ST}$, the black dashed line, $ENAW_{SP}$
557 and the black box MEDW (acronyms defined in text). The contours sloping up toward the right
558 of the plot show potential density and down to the right of the plot show selected spice levels. On

559 panel (b) the two circles highlight water sourced on the shelf (red) and within the salinity cores
560 (black) at 110 m depth, during equatorward slope current flow.

561 Figure 5:

562 Time mean transects between 24th July and 5th August, during which time the slope current was
563 equatorward. The transects are from line 1 and glider 330 (a-b) and line 2 and glider 194 (c-d).
564 (a) and (c) are salinity, (b) and (d), temperature. The black contours indicate the density. The
565 lowest line on each plot ((c)-(d)) is the bathymetry at the shelf-break, with the canyons A and B
566 (Figure 1) labelled.

567 Figure 6:

568 The individual salinity transects along line 2, from glider 194 (a) – (f), the salinity profiles (g)
569 and temperature profiles (h) through each of these at 48.55^{o}. The solid lines (g) – (h) indicate
570 transects (a) – (c) and the dashed, (d) – (e), the heavy lines show the mean profiles. The arrow
571 above each plot shows the relevant slope current direction.

572 Figure 7:

573 The salinity along the 1027 kgm^{-3} isopycnal on transect 2 during an equatorward slope current
574 (grey lines) and a poleward slope current (black lines). The individual transects are shown by the
575 dotted lines (in the appropriate color for the slope current direction) and the mean transects for
576 each slope current direction are shown by the heavy, solid lines This isopycnal is highlighted by
577 the heavy black contour in Figures 5 and 8 ((d) – (f)).

578 Figure 8:

579 Time mean transects between 5th August and 15th August, during which time the slope current
580 was poleward. The transects are from transect 1 and glider 330 (a-b) and transect 2 and glider
581 194 (c-d). (a) and (c) are salinity, (b) and (d), temperature. The black contours indicate the

582 density and the lowest line on each plot ((c)-(e)) is the bathymetry at the shelf-break, with the
583 canyons A and B (Figure 1) labelled.

584 Figure 9:

585 The time mean salinity on line 1 averaged between the 31st October 2012 and the 28th of
586 November 2012. The contours show potential density

587 Figure 10:

588 (a) Potential density profiles of Nitrate + Nitrite at 4 points along the Petite Sole canyon (C1:C4,
589 where C1 is on the shelf and C4 at the mouth of the canyon). The solid lines indicate the
590 background shelf density (27 kg m^{-3}) and the density within the salinity cores (27.1 kg m^{-3}), with
591 N+N values recorded from the mid point of the 4 profiles. (b) Nitrate + Nitrate at the same 4
592 points in the canyon and on the shelf, shelfward of the canyon (shelf). The dashed line indicate
593 the maximum upwelling depth and the depth of the center of the salinity cores, the yellow dots
594 show where the C4 and shelf profiles intersect the y-axis.

595 Table 1:

596 The instruments and sensors used within this study their locations (with reference to Figure 1)
597 and their dates of deployment.

Figure 1. Figure

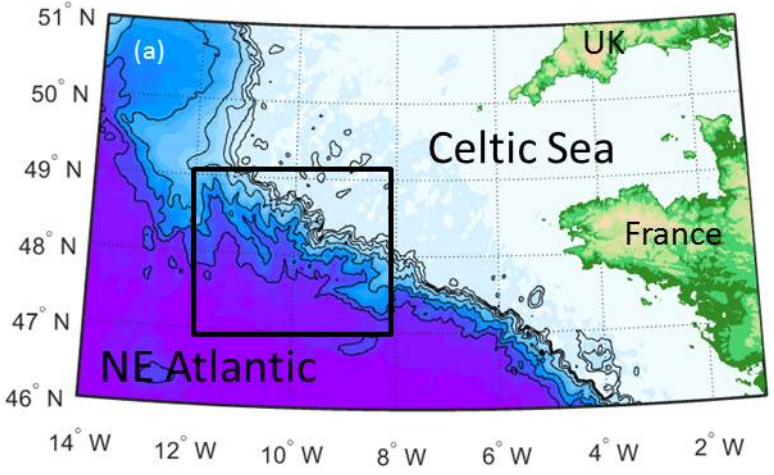
(a)
UK
Celtic Sea
France
NE Atlantic
51° N
50° N
49° N
48° N
47° N
46° N
14° W
12° W
10° W
8° W
6° W
4° W
2° W

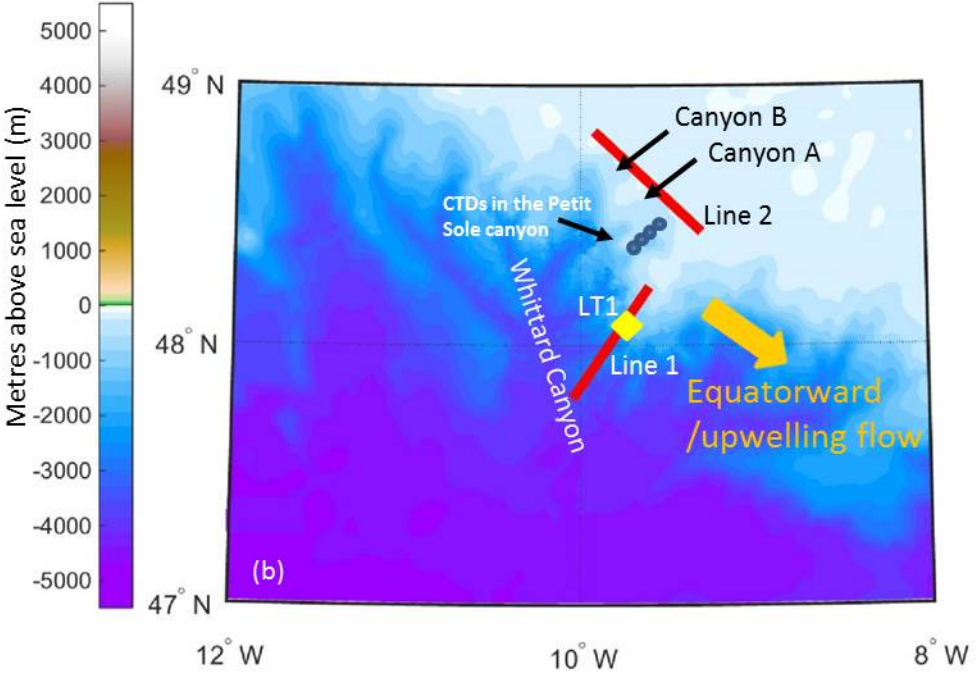
Metres above sea level (m)
5000
4000
3000
2000
1000
0
-1000
-2000
-3000
-4000
-5000
49° N
48° N
47° N
12° W
10° W
8° W
Canyon B
Canyon A
Line 2
CTDs in the Petit Sole canyon
Whittard Canyon
LT1
Line 1
Equatorward /upwelling flow
(b)

Figure 2. Figure

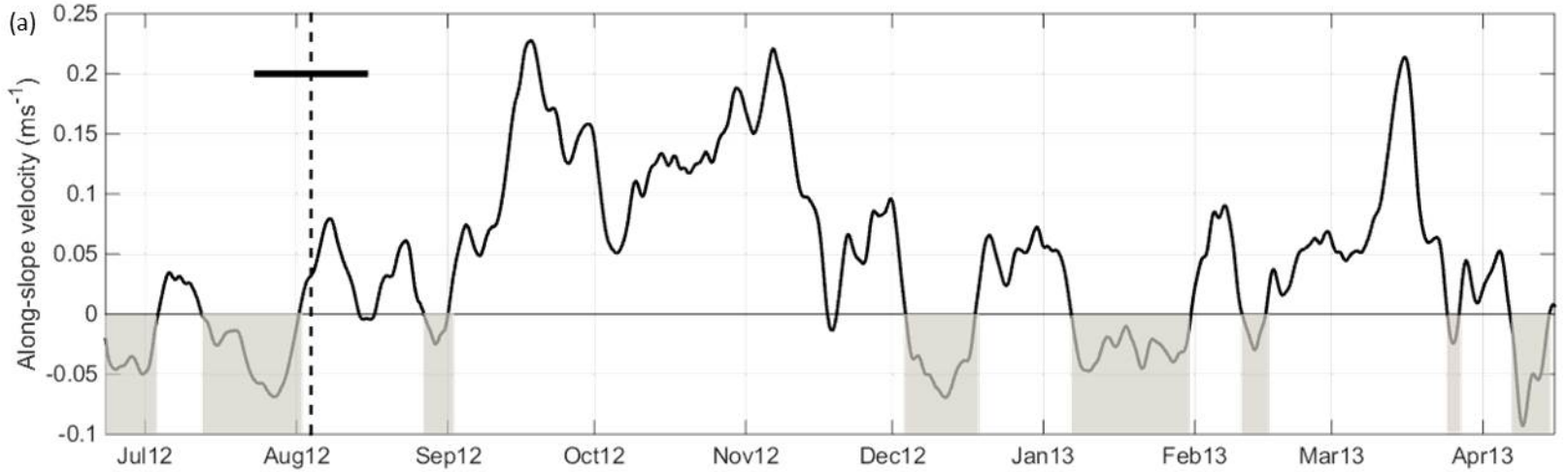
(a)
Along-slope velocity (ms-1)
0.25
0.2
0.15
0.1
0.05
0
-0.05
-0.1
Jul12
Aug12
Sep12
Oct12
Nov12
Dec12
Jan13
Feb13
Mar13
Apr13

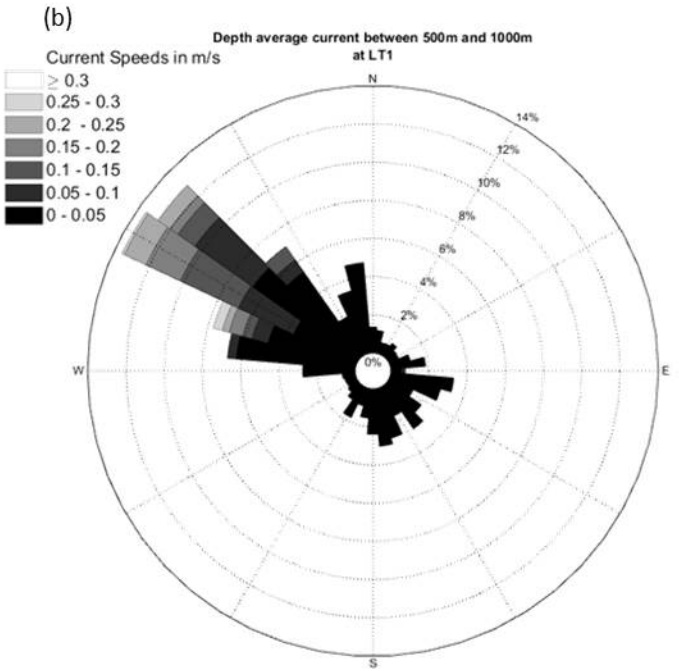
(b)
Depth average current between 500m and 1000m
at LT1
Current Speeds in m/s
≥ 0.3
0.25 - 0.3
0.2 - 0.25
0.15 - 0.2
0.1 - 0.15
0.05 - 0.1
0 - 0.05
N
E
S
W
14%
12%
10%
8%
6%
4%
2%
0%

Figure 4. Figure

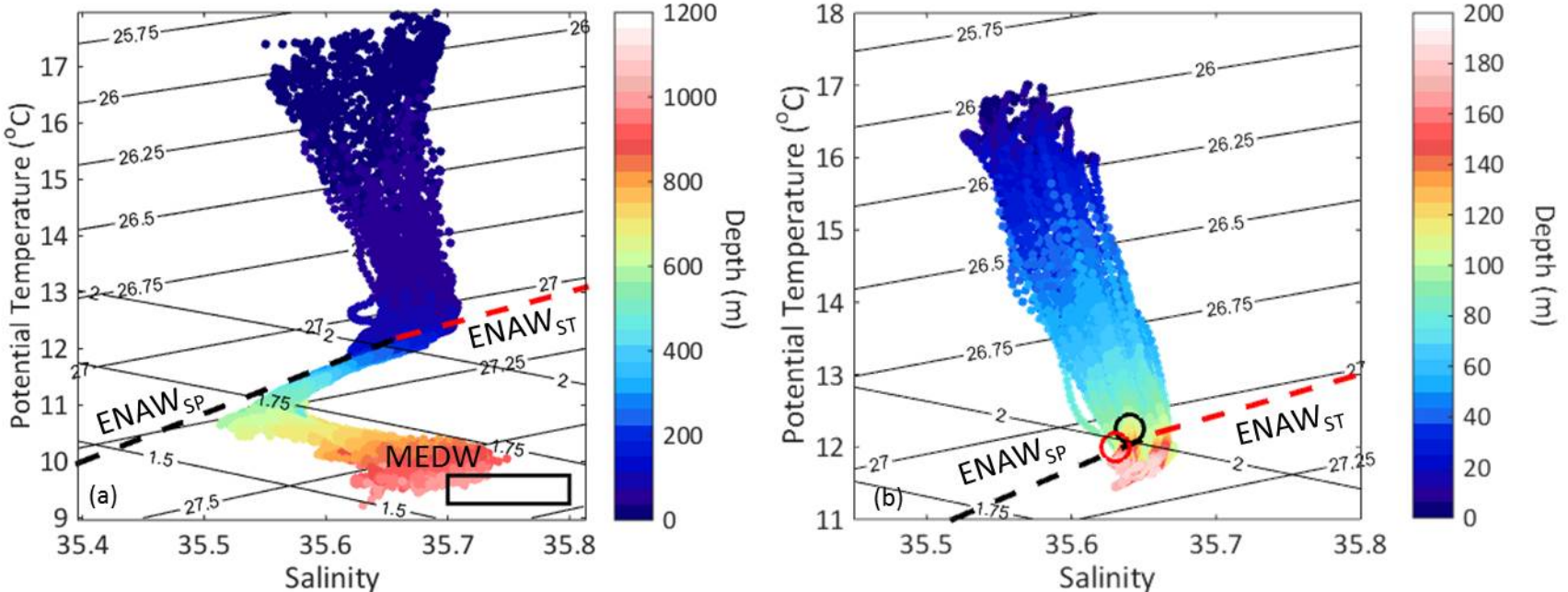
Potential Temperature (°C)
Salinity
Depth (m)
ENAW ST
ENAW SP
MEDW
(a)
(b)

Figure 3. Figure

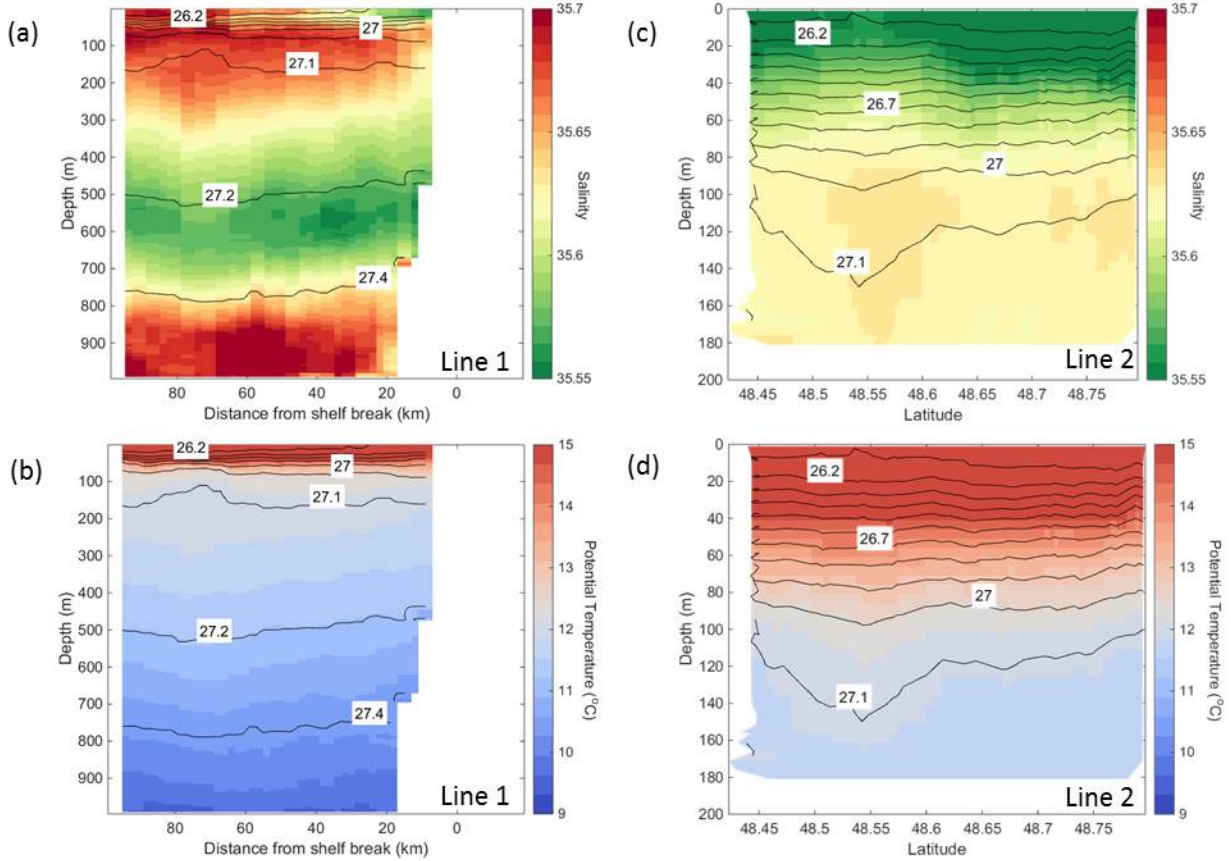
(a)
(b)
(c)
(d)
Depth (m)
Distance from shelf break (km)
Latitude
Salinity
Potential Temperature (°C)
Line 1
Line 2
26.2
27
27.1
27.2
27.4
26.7

Figure 5. Figure

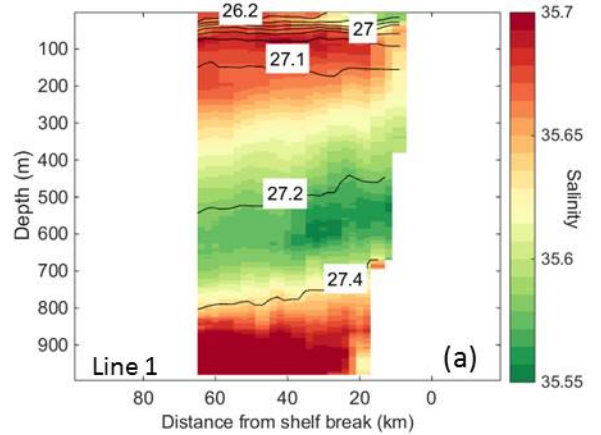
26.2
27
27.1
27.2
27.4
Line 1
(a)
Depth (m)
Distance from shelf break (km)
Salinity
35.7
35.65
35.6
35.55

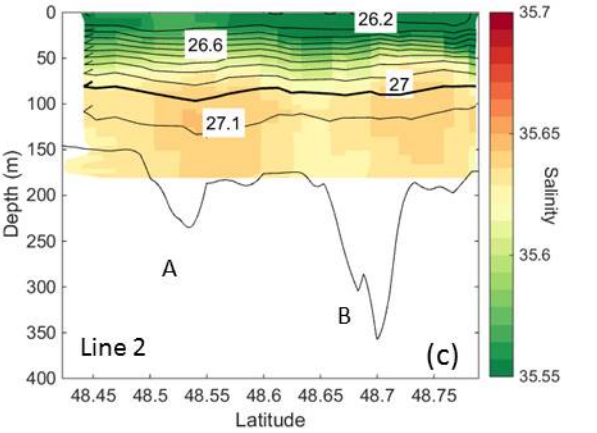
26.2
26.6
27
27.1
A
B
Line 2
(c)
Depth (m)
Latitude
Salinity
35.7
35.65
35.6
35.55

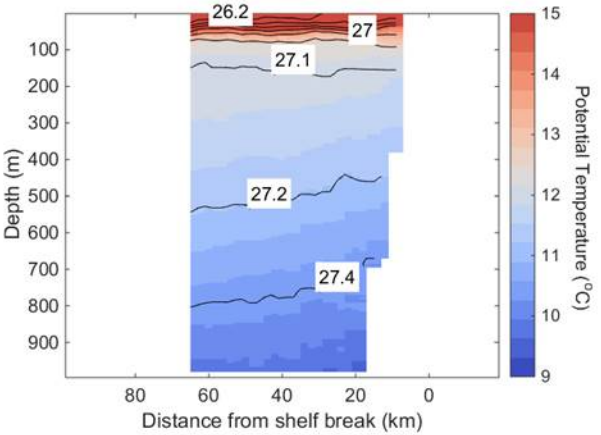
26.2
27
27.1
27.2
27.4
Depth (m)
Distance from shelf break (km)
Potential Temperature (°C)

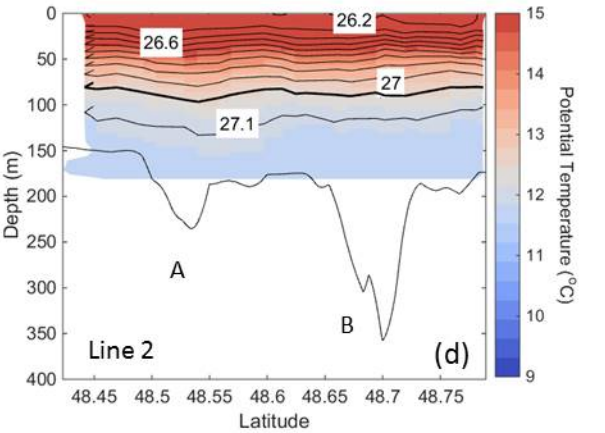
26.2
26.6
27
27.1
A
B
Line 2
(d)
Depth (m)
Latitude
Potential Temperature (°C)

Figure 6. Figure

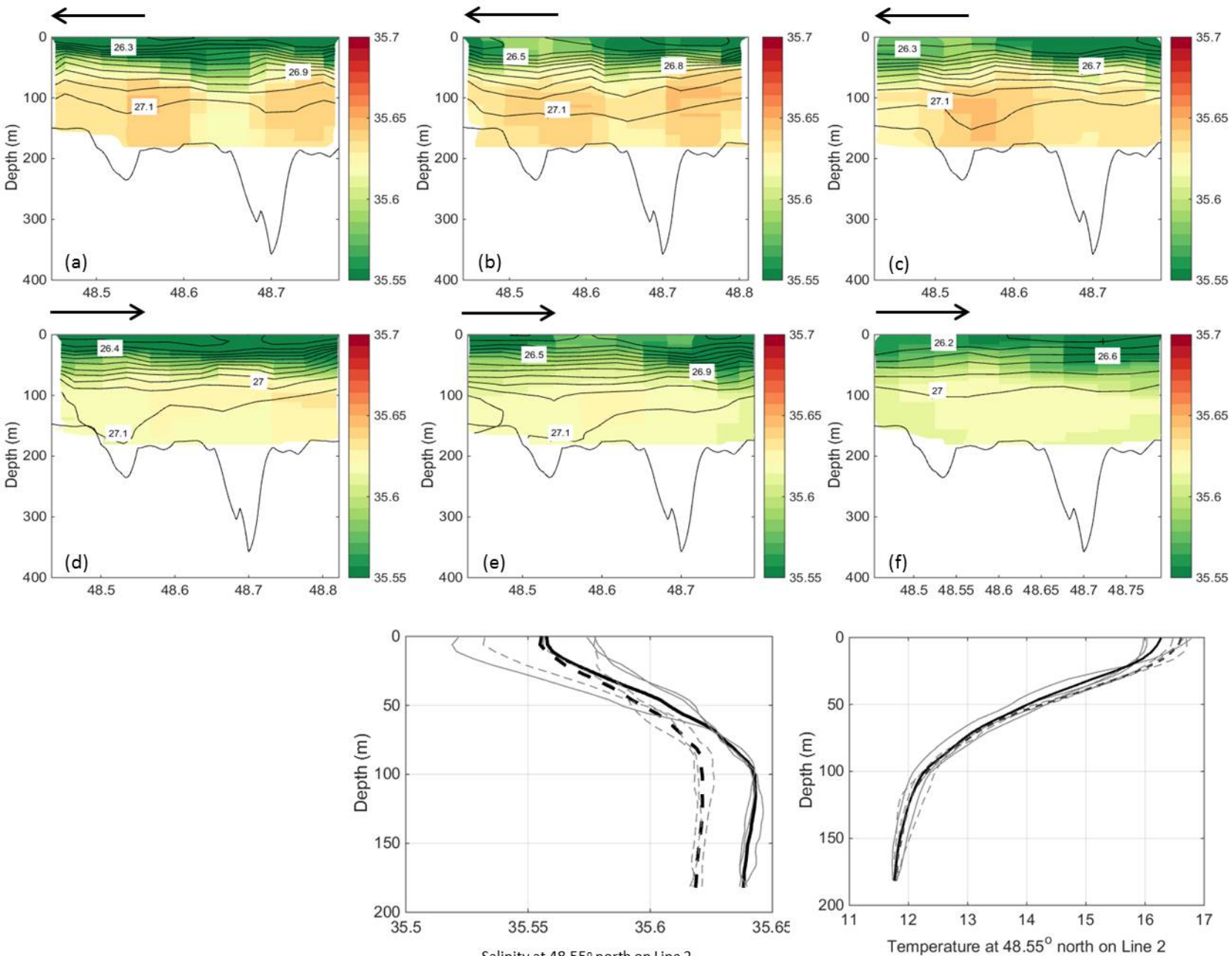
(a)
(b)
(c)
(d)
(e)
(f)
Depth (m)
26.3
26.9
27.1
26.5
26.8
26.7
26.4
27
26.2
26.6
35.7
35.65
35.6
35.55
Salinity at 48.55° north on Line 2
Temperature at 48.55° north on Line 2

Figure 7. Figure

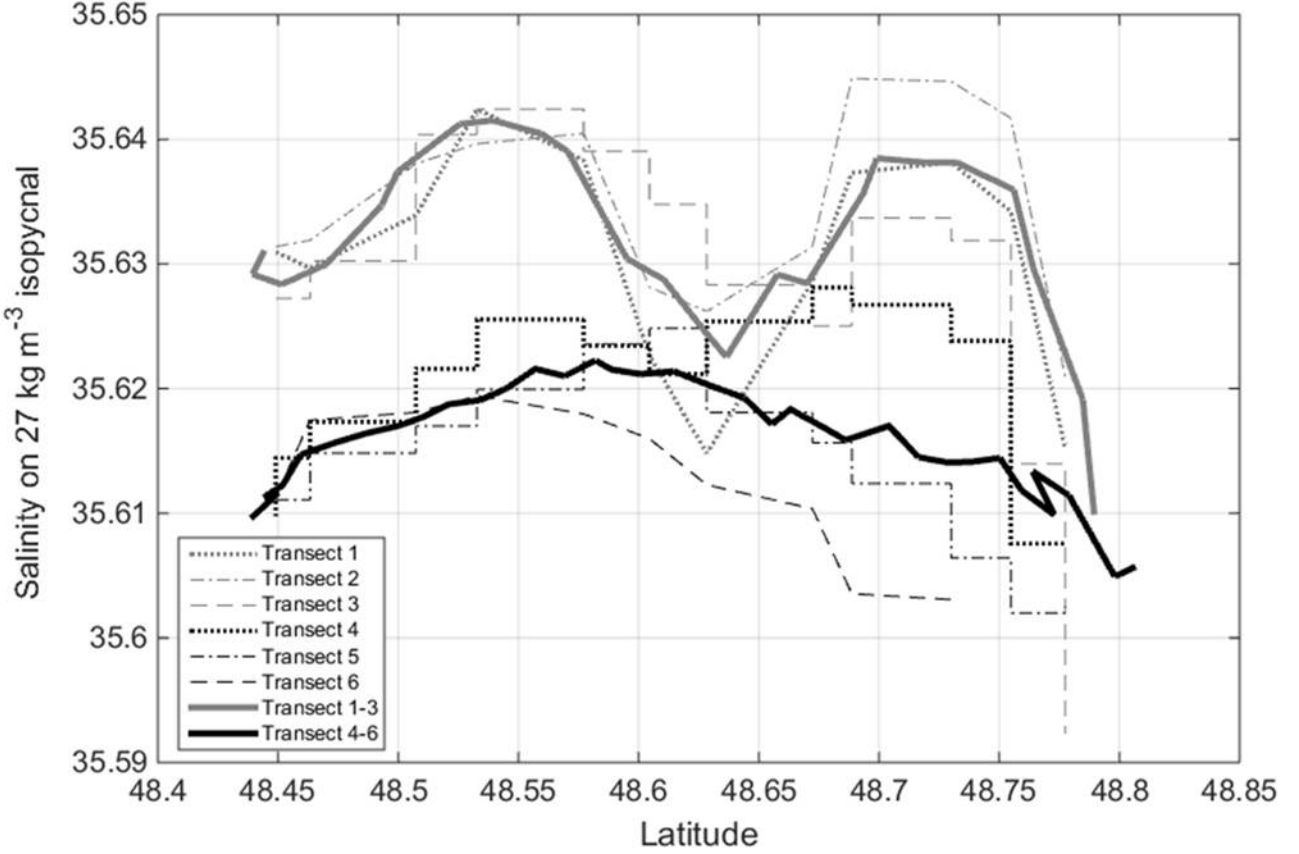
35.65
35.64
35.63
35.62
35.61
35.6
35.59
Salinity on 27 kg m-3 isopycnal
48.4
48.45
48.5
48.55
48.6
48.65
48.7
48.75
48.8
48.85
Latitude
Transect 1
Transect 2
Transect 3
Transect 4
Transect 5
Transect 6
Transect 1-3
Transect 4-6

Figure 8. Figure

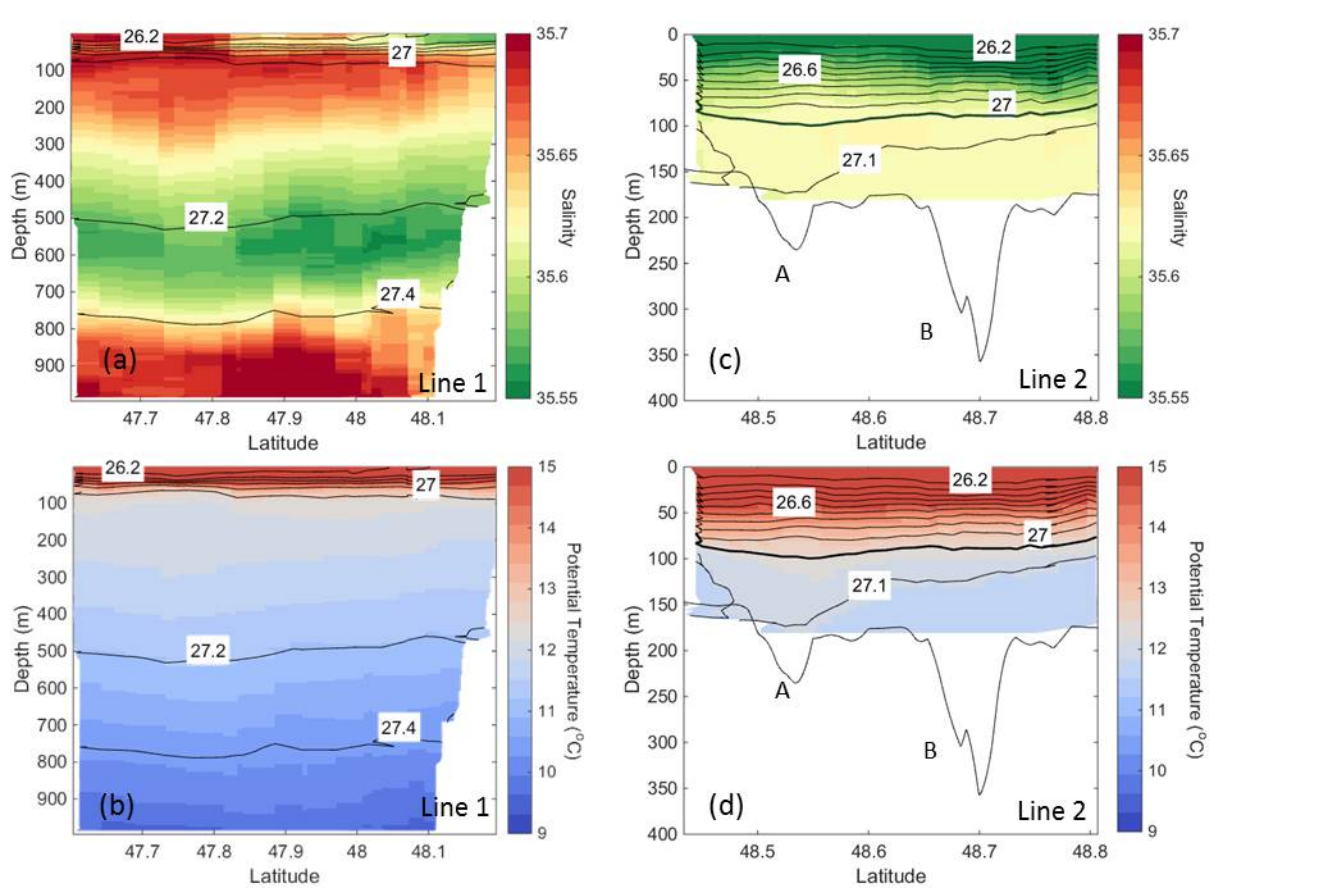
(a)
Line 1
26.2
27
27.2
27.4
Depth (m)
Latitude
Salinity
(b)
Line 1
Potential Temperature (°C)
(c)
Line 2
26.6
27.1
A
B
(d)
Line 2

Figure 9. Figure

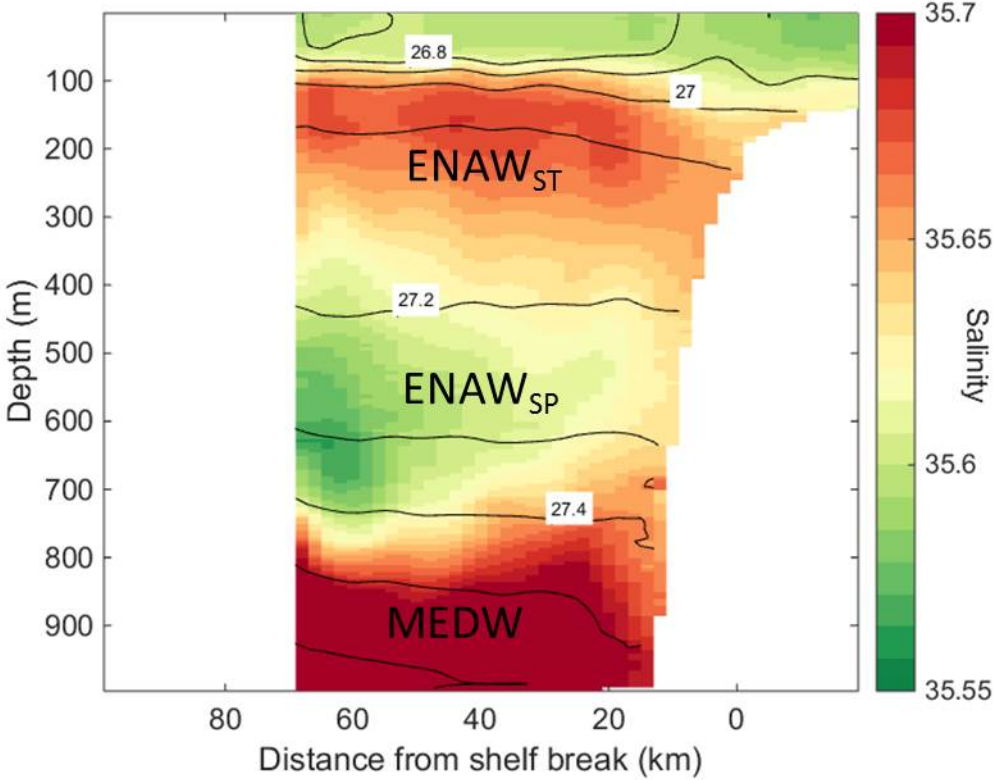
26.8
27
27.2
27.4
ENAW$_{ST}$
ENAW$_{SP}$
MEDW
Depth (m)
100
200
300
400
500
600
700
800
900
80
60
40
20
0
Distance from shelf break (km)
35.7
35.65
35.6
35.55
Salinity

Figure 10. Figure

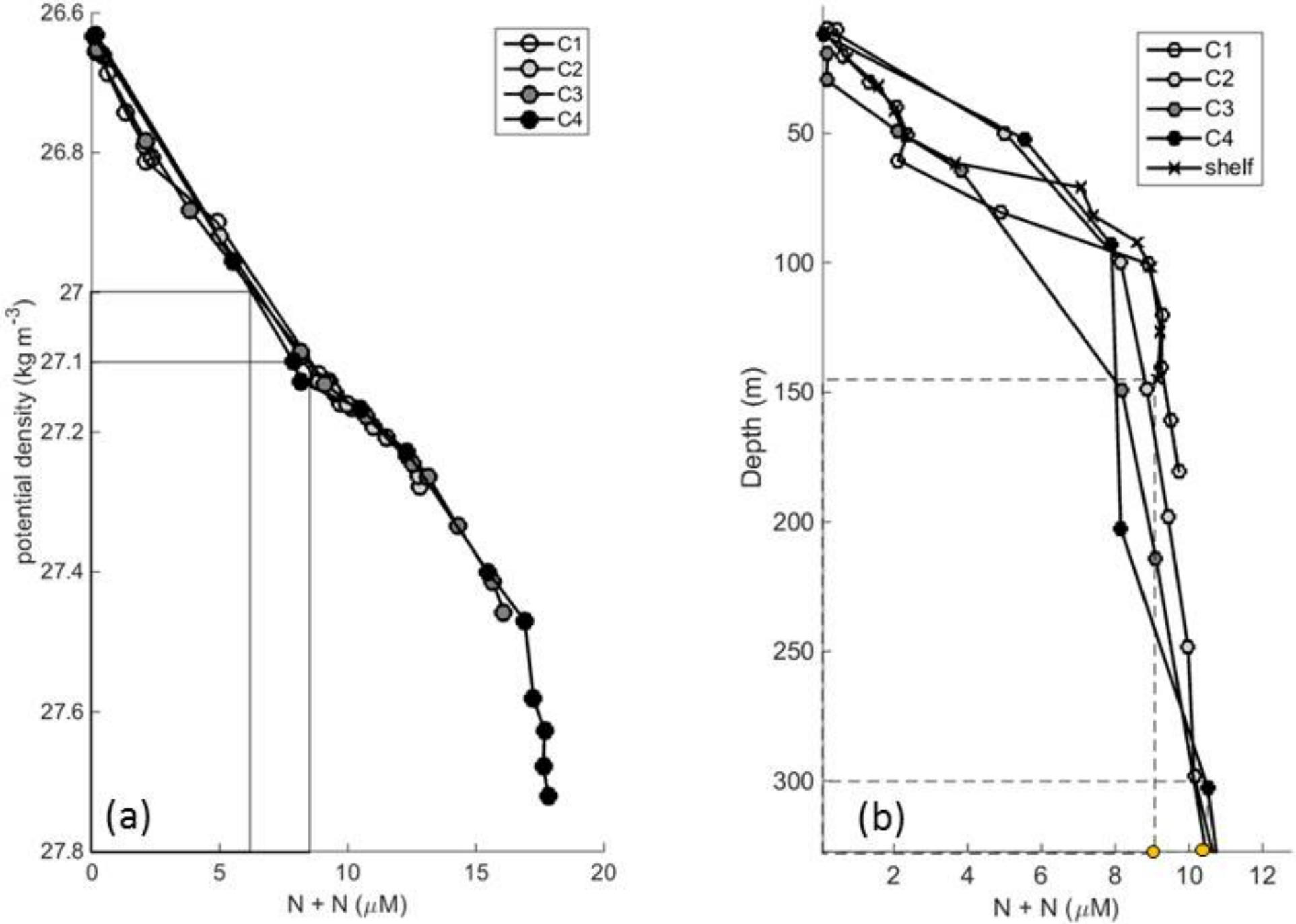
26.6
26.8
27
27.1
27.2
27.4
27.6
27.8
potential density (kg m-3)
C1
C2
C3
C4
(a)
0
5
10
15
20
N + N (μM)
50
100
150
200
250
300
Depth (m)
C1
C2
C3
C4
shelf
(b)
2
4
6
8
10
12
N + N (μM)

Instrument	Sensor	Occupation location
		(referencing Figure 1)
Slocum glider (SN 330)	CTD - SBE 41	Line 1
Slocum glider (SN 194)	CTD - SBE 41	Line 2
Seaglider (sg156)	CTD - SBE-3 and SBE-4	Line 1
ADCP	75kHz RDI ADCP and 75kHz Flowquest ADCP	LT1
CTD rosette	SBE-3 and SBE-4	PS canyon

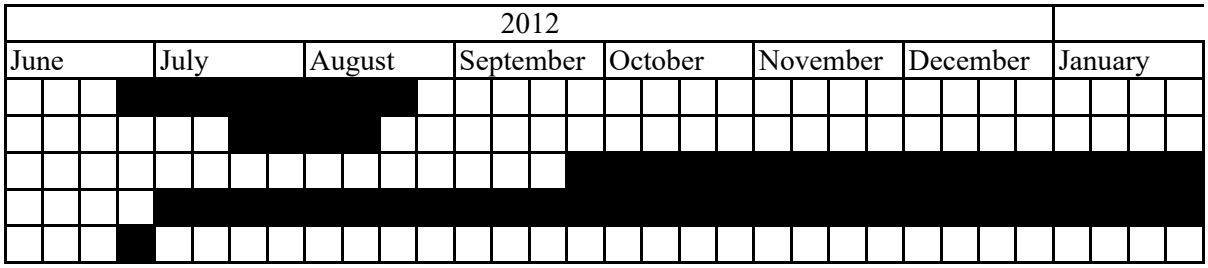
2012
June
July
August
September
October
November
December
January

2013											
February				March				April			